Research Square

Preprints are preliminary reports that have not undergone peer review.
They should not be considered conclusive, used to inform clinical practice,
or referenced by the media as validated information.

A Study on Parameter Estimation for Low-Altitude Small UAVs Target Based on RSPWVD-CFD

Siqi Peng

003058@peihua.edu.cn

Xi'an Peihua University

Article

Keywords: Rotary-wing UAV, Micro-Doppler, RSPWVD, CFD, Micro-motion parameter estimation

Posted Date: November 26th, 2026

DOI: https://doi.org/10.21203/rs.3.rs-11593297/v1

License: This work is licensed under a Creative Commons Attribution 4.0 International License.
Read Full License

Additional Declarations: No competing interests reported.

A Study on Parameter Estimation for Low-Altitude Small UAVs Target Based on RSPWVD-CFD

Siqi Peng[1,*]

1.School of Intelligent Science and Engineering, Xi’an Peihua University, Xi’an 710125, China; 003058@peihua.edu.cn;
*Correspondence: 003058@peihua.edu.cn;

ABSTRACT

Noise interference and blurred micro-Doppler trajectories limit the accurate estimation of rotorcraft UAV micro-motion parameters. To address these challenges, this paper proposes an RSPWVD-CFD-based parameter estimation method. First, a dynamic radar echo model is established that accounts for the UAV’s spatial geometry, rotor micro-vibration effects, and interference from the main body’s motion; Subsequently, the rearranged smoothed pseudo-Wigner-Ville distribution (RSPWVD) is employed to perform high-resolution time-frequency analysis of the echo signals. Combined with the Cadence Frequency Diagram (CFD), the rotor blade flutter frequency is extracted, and the maximum micro-Doppler frequency is estimated via maximum value search, thereby enabling the inversion of micro-motion parameters such as rotor speed and blade length. The effectiveness of the proposed method was verified using simulated quadcopter radar echoes under hovering and constant-velocity motion, with SNR values ranging from −10 to 25 dB and 100 Monte Carlo trials per SNR condition. The time-frequency representation was compared with STFT, WVD, and SPWVD. The results show that this method can accurately extract rotor micro-Doppler characteristics, with reported relative root-mean-square errors (RMSEs) of 0.25% and 2.65% for rotational speed and blade length under hovering conditions, and 0.38% and 3.12% under moving conditions, respectively. When the SNR exceeds 0 dB, both errors remain below 4% in the hovering case and 6% in the moving case under the considered simulation settings.

Keywords: Rotary-wing UAV; Micro-Doppler; RSPWVD; CFD; Micro-motion parameter estimation

Introduction

With the rapid development of drone technology, small rotorcraft drones—thanks to their simple structure, low cost, ease of operation, and portability—have found extremely widespread application in many fields, including military reconnaissance, logistics and transportation, aerial photography and surveying, and agricultural and forestry pest control. However, the explosive growth in the number of drones has also brought significant airspace safety risks. In particular, frequent incidents of “unauthorized flights” and flight disruptions involving certain “low, slow, and small” (low-altitude flight, slow movement, and small radar cross-section) rotorcraft drones in airport airspace exclusion zones, military restricted areas, or critical sensitive areas pose a serious threat to the safety of civil aviation passenger aircraft takeoffs and landings, as well as to national public safety. Consequently, how to achieve effective surveillance, detection, and precise identification of low, slow, and small rotorcraft UAVs has become a pressing and challenging issue in the fields of radar-based collaborative control and security defense, both domestically and internationally [1]. Recent studies have investigated energy-constrained cooperative path planning, multi-objective coordination, and adaptive coverage scheduling for heterogeneous unmanned systems in complex environments [29-31]. These developments emphasize the importance of reliable environmental perception and motion-related information. In contrast, the present study focuses on radar-based estimation of UAV rotor micro-motion parameters.

Among the various detection methods, radar has become the primary means of detecting low, slow, and small UAVs due to its unique advantages, including all-weather, all-time, and long-range detection capabilities, as well as its ability to accurately obtain information on target motion dynamics. However, because rotorcraft UAVs are small and typically made of composite materials, their radar cross-section (RCS) is usually small. Furthermore, due to their slow translational velocity, their echo signals are easily masked by strong ground clutter or environmental noise. Fortunately, during flight or hovering,

the rapid rotation of a UAV's rotor blades induces an additional periodic frequency modulation effect on its primary radar echo; this phenomenon is known in academia as the micro-Doppler effect [2]. Micro-Doppler characteristics, serving as "fingerprint" features for radar target identification and classification, can precisely characterize the target's microscopic motion geometry, such as key physical parameters including rotor speed, number of blades, and blade length [3]. Through in-depth analysis and extraction of the micro-Doppler characteristics of low, slow, and small UAVs, it is possible to effectively distinguish UAVs from interfering targets such as birds and clutter, thereby providing a solid physical and theoretical foundation for target attribute determination and refined classification and identification [4].

Due to the highly non-stationary, time-varying nature of radar echo signals from rotorcraft drones, as well as the severe coupling among their multiple components, traditional Fourier transforms struggle to capture the trajectory of their instantaneous frequency changes. Therefore, it is necessary to employ joint time-frequency analysis methods to conduct detailed observations of micro-motion characteristics in the time-frequency domain [7]. The Short-Time Fourier Transform (STFT), as the most classical and computationally efficient linear time-frequency analysis method, does not suffer from troublesome cross-term interference. However, due to the Heisenberg uncertainty principle (which dictates that time and frequency resolutions are mutually exclusive), it cannot simultaneously achieve high time resolution and high frequency resolution, resulting in severely blurred micro-Doppler trajectories in time-frequency plots [8]. In contrast, the Wigner-Ville distribution (WVD), as a typical quadratic time-frequency distribution, offers extremely high time-frequency concentration and spatial resolution for single-component signals [9]. However, for multi-component radar signals from multi-rotor UAVs, the WVD introduces severe quadratic cross-term interference during computation. These spurious cross-term components completely overwhelm the true micro-Doppler modulation trajectories of the rotors, rendering subsequent parameter extraction ineffective. To suppress these cross-terms while improving time-frequency resolution, researchers have introduced improved methods such as compressed sensing time-frequency analysis [10] and the Smoothed Pseudo-Wigner-Ville Distribution (SPWVD). However, when processing highly noisy and coupled multi-rotor signals, these methods still suffer from issues such as excessive computational complexity, time-frequency energy divergence, and loss of signal details.

To fundamentally address the challenge faced by traditional time-frequency analysis methods—namely, the difficulty of balancing time-frequency resolution with cross-term suppression—time-frequency post-processing methods have emerged. The Reassigned Spectrogram (RSP) significantly enhances the energy concentration of time-frequency spectra and effectively removes some blurring artifacts by redistributing energy within local time-frequency regions to their energy centers [11]. Since then, reassignment methods have been extensively studied in the processing of non-stationary signals and in the extraction of micro-Doppler features from speech and radar signals [12-13]. At the same time, a series of algorithms based on the concept of time-frequency energy reassignment and focusing—such as the Synchrosqueezing Transform (SST) and the Synchroextracting Transform (SET)—have also demonstrated excellent instantaneous frequency resolution by squeezing time-frequency energy along the frequency axis [14-15]. In the field of radar, to simultaneously achieve the high resolution of the WVD and the compactness of the joint time-frequency distribution, a rearrangement operator was introduced into the smoothed pseudo-Wigner-Ville distribution, forming the rearranged smoothed pseudo-Wigner-Ville distribution (RSPWVD) framework. This method uses a time-frequency smoothing window to filter out the vast majority of multicomponent cross-terms in the preliminary stage, and then employs a rearrangement mechanism to re-converge the time-frequency energy—which has diverged due to window function smoothing—back to the true instantaneous frequency center. Consequently, it achieves highly concentrated, micro-Doppler representations with reduced cross-term interference in complex environments where signals from multiple rotors and blades are intertwined [16-17].

After acquiring high-resolution time-frequency images, another core task is to robustly estimate the physical parameters of the rotor (such as rotational speed and blade length). When a rotor blade rotates to a position perpendicular to the radar antenna's line of sight, all scattering points exhibit the same Doppler shift, resulting in a high-energy "blade flash" pulse

signal on the time-frequency image. The periodicity of this blade flash phenomenon—or micro-Doppler feature—can be captured by applying a Fourier transform to the time-frequency matrix along the time dimension. The resulting diagram is known as a cadence frequency diagram (CFD), which is used to precisely extract the blade's flash frequency (i.e., the cadence frequency) [18-19]. Based on this approach, He Weikun et al. [20] proposed the RSP-CFD feature extraction method, which achieves accurate inversion of micro-vibration characteristics in small rotor-based UAVs by estimating maximum value parameters based on rearranged spectra; Chen Xiaokai et al. [21] further explored robust estimation of rotor parameters under low signal-to-noise ratios based on localized synchronous compression or time-reversible localized transforms (such as the TELSET algorithm); Ge Lihao et al. [22] conducted in-depth research on the effectiveness of rearranged spectra in refined feature matching and recognition for UAVs by combining the RSPWVD algorithm. Unlike RSP-CFD [20] and TELSET [21], this study integrates SPWVD-based reassignment (Equations (19)–(21)) with CFD-based parameter inversion (Equations (33)–(39)). Compared with the RSPWVD-based recognition approach in [22], the present study further considers translational motion (Equations (2)–(7)) and focuses on rotor speed and blade length estimation. Nevertheless, existing methods still face challenges in balancing time-frequency concentration, interference suppression, and accurate rotor parameter estimation under translational motion. Therefore, this study investigates an integrated RSPWVD-CFD framework for rotor speed and blade length estimation under hovering and moving conditions. It is worth noting that current deep learning-based target recognition networks [23-24] and intelligent target/motion detection models based on the YOLO (You Only Look Once) series [25] have demonstrated a very high level of automation in UAV radar spectrogram classification, aerial remote sensing, and feature detection [26-28]. However, deep learning networks rely heavily on massive amounts of labeled data, and their "black-box" nature lacks physical interpretability. In contrast, directly inverting the physical parameters of the rotor using explicit, high-resolution signal processing algorithms (such as RSPWVD-CFD) not only enables highly targeted computations but also yields physical features—such as rotational speed and blade length—that possess unparalleled intuitiveness and robustness.

To address the issues of blurred time-frequency trajectories and a raised CFD spectral baseline—which lead to reduced parameter estimation accuracy in existing extraction methods when operating in low signal-to-noise ratio environments or when the UAV body is subject to translational disturbances—this paper proposes an RSPWVD-CFD-based method for estimating micro-motion parameters of rotorcraft UAVs. This method first constructs a dynamic radar echo model that comprehensively accounts for the geometric topology of multi-rotor systems, the randomness of initial rotation phases, and spatial translational disturbances from the UAV body; Subsequently, the RSPWVD algorithm is applied to perform time-frequency focusing on the echo signals, achieving high-energy convergence of micro-Doppler trajectories while completely eliminating multi-component and multi-blade cross-terms; CFD analysis is then introduced based on the time-frequency matrix to extract a robust blade flutter frequency along the time dimension for inverting the rotor speed; Finally, the maximum micro-Doppler shift is located by searching for boundary maxima in the time-frequency plot, and the blade length is calculated. The main contributions of this study are summarized as follows: (1) A multirotor radar echo model incorporating rotor geometry, blade micro-motion, and constant radial motion is formulated. (2) An integrated RSPWVD-CFD procedure is established to estimate rotor speed and blade length using cadence-frequency features and maximum micro-Doppler frequency. (3) The parameter estimation performance is examined under hovering and constant-velocity motion across different SNR conditions.

General Approach

Addressing the issues of strong non-stationarity and multi-component coupling in the radar echo signals of low-altitude, slow-flying, small rotorcraft UAVs—as well as the difficulty of traditional time-frequency analysis methods in balancing time-frequency resolution with cross-term suppression—this paper proposes a method for estimating micro-Doppler parameters of rotorcraft UAVs based on RSPWVD-CFD. Based on a radar echo model for rotorcraft UAVs, this method combines Rearranged Smoothed Pseudo-Wigner-Ville Distribution (RSPWVD) with Cadence Frequency Diagram (CFD) analysis to achieve high-precision extraction of micro-Doppler features and estimation of key rotorcraft parameters.

This method first establishes a dynamic radar echo model that accounts for the spatial geometry of the UAV and the micro-vibration effects of the rotors, thereby generating simulated echo signals with typical micro-Doppler modulation characteristics. Subsequently, RSPWVD is used to perform high-resolution time-frequency analysis on the echo signals; through a rearrangement mechanism, the energy concentration in the time-frequency domain is enhanced to obtain clear and continuous micro-Doppler trajectories; Furthermore, CFD is used to perform a Fourier transform of the time-frequency matrix along the time dimension to extract the rotor blade flutter frequency, and this is combined with a search for maxima in the time-frequency plot to estimate the maximum micro-Doppler frequency; finally, based on the theoretical relationship between the blade flutter frequency and the maximum micro-Doppler frequency, key micro-motion parameters such as rotor speed and blade length are inversely estimated.

The overall research approach is shown in Figure 1.

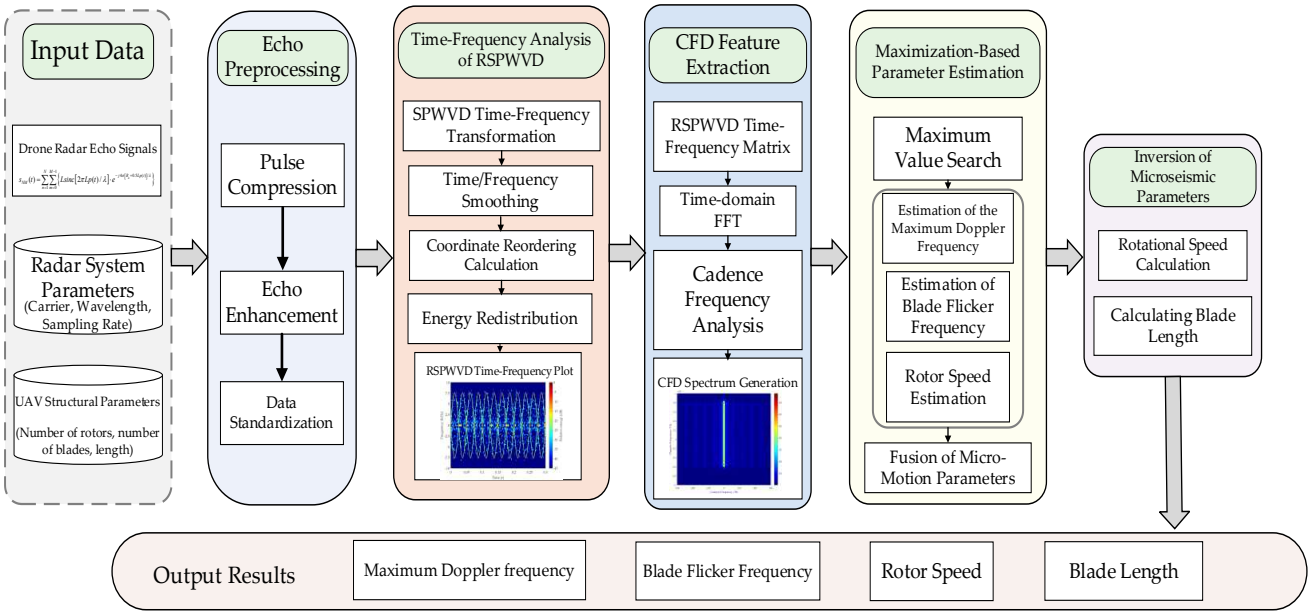

Fig. 1. Overall Framework for Extracting Micro-motion Parameters of Rotorcraft UAVs Based on RSPWVD-CFD

According to Figure 1, the specific processing workflow of the proposed RSPWVD-CFD method is as follows:

(1) Modeling of UAV rotor radar echoes: A radar echo model is established that accounts for the UAV's spatial geometry and the micro-motion effects of the rotor blades. Simulated echo signals with typical micro-Doppler characteristics are generated, providing a data foundation for subsequent time-frequency analysis and parameter estimation.

(2) RSPWVD time-frequency analysis and CFD feature extraction: RSPWVD is used to perform high-resolution time-frequency analysis of the radar echo, enhancing time-frequency energy concentration and suppressing cross-term interference; based on this, an FFT transform is applied to the time-frequency matrix along the time dimension to construct a CFD spectrum and extract periodic features such as the blade flutter frequency.

(3) Micro-motion Parameter Estimation: The maximum value search method is used to estimate the maximum micro-Doppler frequency in the time-frequency plot and the blade flutter frequency in the CFD spectrum, respectively. Based on the theoretical relationship between the two, key micro-motion parameters—such as rotor speed and blade length—are inverted, enabling high-precision estimation of micro-motion parameters for rotor-based UAVs.

A Method for Time-Frequency Analysis of Echo Signals from Low-Altitude, Slow-Flying, Small Drones

3.1 *Modeling of Echo Signals from Low-Flying, Slow-Moving, Small Drones*

Currently, mainstream light and small unmanned aerial vehicles (UAVs) share a high degree of similarity in their overall structural layout, consisting primarily of a central airframe and multiple sets of rotating propellers. However, different models vary in specific parameters such as rotor speed, number of blades, and blade length. Different kinematic characteristics manifest unique modulation features in radar echoes. Therefore, this section delves into the distinct micro-vibration characteristics of different UAV rotors and constructs a highly robust mathematical model of rotor radar echoes, providing a theoretical foundation for subsequent signal analysis and micro-vibration feature extraction.

Taking a quadrotor dual-blade UAV as an example, Figure 2 depicts the three-dimensional spatial relative geometric position relationship between the target and the radar. In the established radar measurement coordinate system, the radar is placed at the origin O, the center coordinates of the UAV are O_c, and the rotation axis of its nth rotor is defined as O_n. The azimuth and elevation angles of the target relative to the radar are α and β, respectively, and the spatial geometric distance between the radar center and the target's centroid is R. The main body of the UAV connects the centers of the four rotors, with the equivalent connection length set to d. The initial phase of the nth rotor axis relative to the UAV body is φ_n; the initial phase of the mth blade on the nth rotor is φ_{nm}. The projections of O_c and O_n onto the xOy plane are O_c' and O_n', respectively.

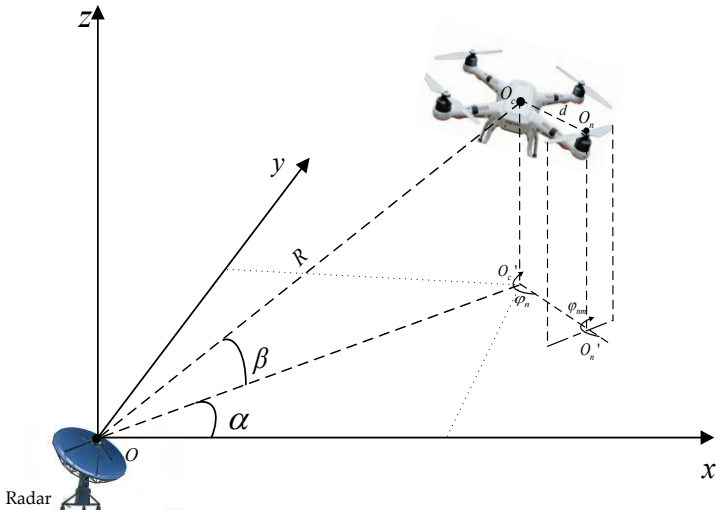

Fig. 2. Relative positions of the drone and the radar

Figure 1. Radar track classification framework integrating statistical features and TCN-SE temporal features

Assuming the UAV is in a hovering state, the spatial geometric distance R_n between the radar center and the axis of the nth rotor is:

$$R_n = \sqrt{R^2 + d^2 + 2Rd\cos\beta\cos(\alpha - \varphi_n)} \quad (1)$$

The square-root operation ensures that R_n has the dimension of length, consistent with its use in the subsequent echo-phase equations.

Set the rotation frequency of the nth rotor of the drone to f_n, the blade length be L, the center carrier frequency of the radar transmitted signal be denoted as f_c, the wavelength be λ, and the speed of light be c. Let σ be the complex scattering coefficient of scattering point P, containing information on scattering intensity and initial phase. Consider an arbitrary ideal scattering point P on the blade of the nth rotor, with its distance from the rotor center being l_p. The instantaneous propagation distance $R_p(t)$ from the scattering point P to the radar can then be expressed as:

$$R_p(t) = R_n + v_r t + l_p p(t) \quad (2)$$

where $p(t) = \cos\beta\cos(2\pi f_n t + \varphi_{nm} + \alpha)$ .For translational motion, v_r denotes the constant radial velocity, with $v_r = 0$ in the hovering case.

Based on electromagnetic scattering theory, the baseband echo signal $s_P(t)$ reflected from scattering point P to the radar is:

$$s_P(t) = \sigma \exp(-j4\pi f_c R_P(t)/c) \quad (3)$$

Substituting Equation (2) into Equation (3) yields:

$$s_P(t) = \sigma \exp(-j4\pi[R_n + v_r t + l_P p(t)]/\lambda) \quad (4)$$

A rotor blade can be regarded as consisting of countless scattering points. Let the length of the blade be . Then, the echo from a single blade can be obtained by integrating along the length of the blade:

$$s_{nm}(t) = \int_0^L s_P(t) dl_P \quad (5)$$

Then, the radar echo signal generated by the mth blade of the nth rotor of the drone is:

$$s_{nm}(t) = Lsinc[2\pi Lp(t)/\lambda]\exp(-j4\pi[R_n + v_r t + 0.5Lp(t)]/\lambda) \quad (6)$$

For a drone with N rotors, each containing M blades, the baseband echo signal received by the radar is:

$$s_{NM}(t) = \sum_{n=1}^{N}\sum_{m=0}^{M-1}\left\{Lsinc[2\pi Lp(t)/\lambda]\cdot\exp(-j4\pi[R_n + v_r t + 0.5Lp(t)]/\lambda)\right\} \quad (7)$$

As can be seen from the total echo analytical expression (7), the total echo signal from a multirotor is mathematically represented as a nonlinear, non-stationary signal consisting of a complex exponential term amplitude-modulated by the $sinc$ function. This model successfully establishes a quantitative relationship between the UAV's spatial geometric configuration, motion state parameters, and radar echo characteristics, providing a solid theoretical basis for analyzing the dynamic micro-Doppler modulation mechanism of the rotors. Due to the signal's highly time-varying and non-stationary nature, traditional frequency-domain analysis methods struggle to effectively separate the multi-component micro-Doppler components. Therefore, the following section introduces the high-resolution time-frequency reordering spectral analysis algorithm (RSPWVD) to achieve a highly coherent representation of micro-Doppler trajectories in the time-frequency domain, thereby laying the foundation for parameter inversion and estimation.

3.2 Time-Frequency Analysis Methods

At present, there are two main categories of time-frequency analysis methods: the first consists of linear time-frequency transforms, such as the short-time Fourier transform (STFT); the second consists of bilinear time-frequency transforms, as represented by the Wigner-Ville distribution (WVD) and the smoothed pseudo-Wigner-Ville distribution (SPWVD).

3.2.1 Short-Time Fourier Transform (STFT)

The STFT is essentially a Fourier transform method that incorporates a windowing mechanism; it is based on the core assumption that a signal is stationary within a short time window. This method obtains the time-frequency distribution of a signal by shifting the window function along the time axis and computing the Fourier transform of the signal within each window segment. The STFT of a time signal can be expressed as

$$STFT(t,f)=\int_{-\infty}^{+\infty}s(\tau)g(t-\tau)e^{-j2\pi f\tau}d\tau \quad (8)$$

In the equation: g(τ) is the smoothing time window; τ is the time delay variable.

As can be seen from Equation (8), the STFT is limited by a fixed time-frequency resolution. While a short window improves time resolution, it sacrifices frequency resolution, and vice versa for a long window. However, the sinusoidal frequency-modulated components within multi-blade echoes require both high time resolution to capture instantaneous frequency evolution and high frequency resolution to distinguish dense spectral lines; this inherent conflict inevitably leads to ambiguity in time-frequency characterization. Furthermore, spectral leakage caused by windowing leads to crosstalk between blade components in the time-frequency domain and further exacerbates spectral aliasing at low pulse repetition frequencies (PRF). For multi-component signals, when the micro-Doppler frequencies of the blades overlap in the time domain, the STFT—due to its lack of adaptive resolution adjustment capabilities—leads to component confusion and makes separation difficult. Its assumption of local stationarity is fundamentally at odds with the strongly non-stationary characteristics of micro-motion signals, and the non-stationarity of the signal within the window inevitably causes feature distortion. In environments with low signal-to-noise ratios, the STFT lacks effective noise suppression mechanisms, making time-frequency plots highly susceptible to being overwhelmed by noise. Furthermore, the selection of window function type and length relies heavily on prior knowledge, thereby losing the flexibility of adaptive adjustment. These theoretical shortcomings collectively limit the accuracy and robustness of the STFT in micro-motion parameter inversion, confining its use to a macroscopic preliminary analysis tool.

The computational load of the STFT depends on the signal length N, the window length L_{win}, the frame shift H_{hop}, and the number of frames K_{frame}, where $K_{frame}=\left[\frac{N-L_{win}}{H_{hop}}\right]+1$ .The total computational complexity is $O\left(K_{frame}\cdot L_{win}\cdot\log_2 L_{win}\right)$.

3.2.2 Wigner-Ville Distribution (WVD)

The WVD is defined as the Fourier transform of the signal's instantaneous auto-correlation function $r_x(t,\tau)$ with respect to the delay variable τ. Its expression is:

$$S_{WVD}(t,f)=\int_{-\infty}^{\infty}r_x(t,\tau)e^{-j2\pi f\tau}d\tau=\int_{-\infty}^{\infty}x\left(t+\frac{\tau}{2}\right)x^*\left(t-\frac{\tau}{2}\right)e^{-j2\pi f\tau}d\tau \quad (9)$$

where $(\cdot)^*$ denotes the complex conjugate.

Since no window function is used, the WVD has a higher time-frequency resolution compared to the STFT. If the signal consists of N_{signal} components,That is $s(t)=\sum_{n=1}^{N_{\text{signal}}}s_n(t)$, it can be decomposed into

$$S_{WVD}(t,f)=\sum_{n=1}^{N_{signal}}WVD_{s_n}(t,f)+\sum_{m=1}^{N_{signal}}\sum_{n\neq m}WVD_{s_m,s_n}(t,f) \quad (10)$$

Among these, item 2 is a cross-term. For multi-blade echoes, the number of cross-terms increases quadratically with the number of blades N_{blade}, making the time-frequency representation complex and confusing.

The total computational load is determined by the signal length N, the maximum delay length L_{maxlag}, and the number of frequency points K_{freq}, that is,

$$O\left(N\cdot\left(2L_{maxlag}+1\right)+N\cdot K_{freq}\cdot\log_2 K_{freq}\right) \quad (11)$$

3.2.3 Smooth Pseudo-Wigner-Wiel Distribution (SPWVD)

To reduce cross-term interference in WVD, a window function is typically applied to smooth the signal. By applying a window function in the time domain, signal autocorrelation terms can be effectively suppressed, thereby deriving PWVD. Building on this, if a window function is further applied in the frequency domain, both autocorrelation and cross-correlation terms can be suppressed, resulting in a smoothed SPWVD distribution. The corresponding mathematical expression can be written as

$$S_{SPWVD}(t,f)=\iint_{-\infty}^{\infty}g(\mu)h(\tau)s\left(t-\mu+\frac{\tau}{2}\right)s^{*}\left(t-\mu-\frac{\tau}{2}\right)e^{-j2\pi f\tau}d\tau d\mu \tag{12}$$

In the equation: $g(\mu)$ is the time-smoothing window; $h(\tau)$ is the lag-smoothing window; $s(t)$ is the original time-domain signal; μ is the time-shift variable.

The time-frequency resolution of SPWVD is limited by the Heisenberg uncertainty principle between the time and frequency smoothing windows: while extending the window length can suppress cross-terms, it tends to cause blurring of the distribution. For multi-blade echoes, the micro-Doppler effects generated by blade rotation require high-resolution tracking of rapid frequency changes. However, the smoothing mechanism of SPWVD leads to main lobe broadening and sidelobe elevation, thereby weakening its ability to capture instantaneous frequency changes. This causes linearly or sinusoidally modulated trajectories to become blurred, making it more difficult to accurately invert blade physical parameters (such as length and rotational speed). Furthermore, in scenarios where multiple blade components overlap, a fixed smoothing window cannot adaptively track rapidly changing instantaneous frequencies, leading to energy diffusion and "trail" effects, which in turn limit the accuracy of feature extraction. These limitations fully expose the inherent shortcomings of SPWVD in analyzing complex multi-component signals.

The computational complexity of SPWVD is $O\left(N\cdot\left(2L_g+4L_g\cdot\tau_{max}+5N_{fft}\log_2\left(N_{fft}\right)\right)\right)$, where N_{fft} is the number of FFT points, L_g is the time-smoothing window length, $\tau_{max}\approx\min\left(\left\lfloor N_{fft}/2\right\rfloor-1,L_h\right)$ is the maximum delay parameter, and L_h is the frequency-smoothing window length.

3.2.4 Time-frequency distributions of the rearranged smooth pseudo-Wigner-Wiel distribution (RSPWVD)

To effectively suppress cross-term interference while maintaining a high level of time-frequency resolution, reordering techniques were adopted and applied to SPWVD, resulting in the development of the redistributed RSPWVD method. The core mechanism of this method lies in optimizing the clarity and accuracy of time-frequency characterization through energy redistribution across the time-frequency plane.

The fundamental basis for the rearrangement operation stems from the mechanism of redistributing the energy distribution of the spectrogram. The spectrogram is defined as the square of the STFT, as shown below:

$$SPEC_x(t,f)=\left|\int_{-\infty}^{\infty}x(u)h^{*}(u-t)e^{-j2\pi fu}du\right|^{2} \tag{13}$$

In the equation: $h(t)$ is the window function. As a bilinear energy distribution function, its spectral plot is similar to that of a conventional WVD distribution; it also suffers from the cross-term problem and does not satisfy the margin property. The WVD distribution has an important property, as shown below:

$$\left|\int_{-\infty}^{\infty}x(t)y^{*}(t)dt\right|^{2}=\int_{-\infty}^{\infty}\int_{-\infty}^{\infty}WVD_x(t,f)WVD_y^{*}(t,f)dtdf \tag{14}$$

Comparing Equation (13) and Equation (14), it can be seen that the left-hand side of Equation (14) bears a strong resemblance to the formula defining the spectrogram. Therefore, the spectrogram can be represented as a two-dimensional convolution of the signal's WVD and the short-time window's WVD:

$$(SPEC_x(t,f) = \int_{-\infty}^{\infty}\int_{-\infty}^{\infty} WVD_x(\tau,v)WVD_h(\tau-t,v-f)d\tau dv \quad (15)$$

In the equation: v is the frequency-delay variable.

The reordering operation calculates the coordinates of the signal's energy center of mass and maps the energy values—which were originally dispersed and accumulated at the geometric center due to the smoothing effect of the window function—back to their true energy center of mass. Specifically, for a given time-frequency point, its reordered center-of-mass coordinates are obtained by performing a weighted integral over its neighborhood using the signal's WVD and the window function's WVD.

Mathematically, the reassigned spectrogram can be viewed as the spatial accumulation result of the original spectrogram values after being remapped according to the centroid coordinate transformation. The formulas for calculating the reassigned time coordinate $\hat{t}(t,f)$ and the reassigned frequency coordinate $\hat{f}(t,f)$ are:

$$\hat{t}(t,f) = \frac{\iint \tau \cdot WVD_h(\tau-t,\xi-f)\cdot WVD_x(\tau,\xi)d\tau d\xi}{SPEC_x(t,f)} \quad (16)$$

$$\hat{f}(t,f) = \frac{\iint \xi \cdot WVD_h(\tau-t,\xi-f)\cdot WVD_x(\tau,\xi)d\tau d\xi}{SPEC_x(t,f)} \quad (17)$$

The value of the reassigned spectrogram at any point (t,f) is equal to the sum of all spectrogram values reassigned to that point. That is, the definition of the reassigned spectrogram is:

$$RSPEC_x(t,f) = \iint SPEC_x(\tau,\xi)\cdot\delta\left(t-\hat{t}(\tau,\xi), f-\hat{f}(\tau,\xi)\right)d\tau d\xi \quad (18)$$

By applying rearrangement techniques to SPWVD, we obtain RSPWVD. SPWVD is defined by Equation (12), and the rearrangement coordinates for RSPWVD are calculated using the corresponding time-frequency weighted distributions:

$$\hat{t}(t,f) = t - \frac{SPWVD_x^{(f)}(t,f)}{2\pi\cdot SPWVD_x(t,f)} \quad (19)$$

$$\hat{f}(t,f) = f + \frac{SPWVD_x^{(t)}(t,f)}{2\pi\cdot SPWVD_x(t,f)} \quad (20)$$

where $SPWVD_x^{(t)}$ and $SPWVD_x^{(f)}$ are the auxiliary weighted distributions associated with frequency and time reassignment, respectively. The reassignment coordinates are obtained from local energy-weighted centroids rather than ordinary derivatives of SPWVD. To avoid numerical instability near zero-energy regions, a threshold-based validity condition is im-

posed: $|SPWVD_x(t,f)| > \varepsilon, \quad \varepsilon = \eta \max_{t,f} |SPWVD_x(t,f)|$. Here, η denotes a predefined relative threshold. For valid time-frequency bins, the reassigned coordinates are discretized using nearest-neighbor mapping: $(i', j') = \left(\text{round}\frac{\hat{t}-t_0}{\Delta t}, \text{round}\frac{\hat{f}-f_0}{\Delta f}\right)$. The corresponding energy values are accumulated at the mapped bins to construct the discrete RSPWVD. The final definition of the RSPWVD is:

$$RSPWVD_x(t,f) = \iint SPWVD_x(\tau,\xi) \cdot \delta\left(t - \hat{t}(\tau,\xi), f - \hat{f}(\tau,\xi)\right) d\tau d\xi \tag{21}$$

3.2.5 Performance Analysis of the Reshuffled Smooth Pseudo-Wigner-Wiel Distribution (RSPWVD)

For a multi-component signal $x(t) = \sum_{k=1}^{K} x_k(t)$ composed of K superimposed components, the traditional WVD generates cross-terms due to its bilinear operation. Its complete decomposition is as follows:

$$WVD_x(t,f) = \sum_{k=1}^{K} WVD_{x_k}(t,f) + 2\sum_{k<l} Re\left\{WVD_{x_k,x_l}(t,f)\right\} \tag{22}$$

Although the SPWVD can suppress cross-terms to a certain extent using time-frequency smoothing windows, it comes at the cost of reduced time-frequency resolution. In contrast, the RSPWVD, by virtue of its reassignment operation, can accurately and inversely concentrate the divergent cross-term energy onto the spatial trajectories where the true signal components lie, achieving, in theory, the complete elimination of cross-terms. Mathematically, cross-terms exhibit strong instability in the reassignment vector field; their computed reassignment coordinates $(\hat{t}, \hat{f})$ differ significantly from those of the true components, thus being effectively dispersed and attenuated during the energy mapping and redistribution process.

Time-frequency concentration is a key metric for evaluating the quality of a time-frequency distribution. It intuitively reflects the degree to which signal energy converges and concentrates around the instantaneous frequency trajectory. The RSPWVD significantly enhances concentration through the reassignment operation. In the RSPWVD, the reassigned coordinate $\hat{f}(t,f)$ serves as an estimate of the instantaneous frequency. Assume the signal can be locally approximated as a linear frequency-modulated signal:$x(t) \approx exp\left(j2\pi\left(f_0 t + \frac{\alpha}{2}t^2\right)\right)$,Its instantaneous frequency is $f_i(t) = f_0 + \alpha \cdot t$ .At this point, there is the following quantitative relationship between the partial derivative term corresponding to SPWVD and the instantaneous frequency:

$$f_{IF}(t) = \frac{1}{2\pi}\frac{d}{dt}\arg x(t) = f_0 + \alpha t \tag{23}$$

Substitute into the formula for rearranged coordinates:

$$\hat{f}(t,f) \approx f_{IF}(t) = f_0 + \alpha t \tag{24}$$

From Equation (24), it can be seen that the reassignment operation moves energy from point (t,f) to $\left(t, f_i(t)\right)$, concentrating the energy onto the instantaneous frequency trajectory under the assumed locally linear frequency modulation conditions.

The edge property requires that the integral of the time-frequency distribution over the time and frequency domains be equal to the signal's energy density. Time edge:

$$\int_{-\infty}^{\infty} TF_x(t,f)df = |x(t)|^2 \tag{25}$$

Frequency Edge:

$$\int_{-\infty}^{\infty} TF_x(t,f)dt = |X(f)|^2 \quad (26)$$

where $TF_x(t,f)$ is the time-frequency distribution function. First, the reassignment operation is energy-conserving, as shown below:

$$\iint RSPWVD_x(t,f)dtdf = \iint SPWVD_x(t,f)dtdf = \|x\|^2 \quad (27)$$

Derivation of the time integral for the RSPWVD:

$$\int RSPWVD_x(t,f)df \approx \int SPWVD_x(\hat{t},f)df \quad (28)$$

This means that the time edge of RSPWVD is the projection of SPWVD onto the rearrangement time coordinate, and the time edge of SPWVD is

$$\int SPWVD_x(t,f)df = |x(t)|^2 * |g(t)|^2 \quad (29)$$

In the equation: g(t) is the time window; * denotes the convolution operation. Due to convolution, SPWVD does not satisfy strict boundary conditions; RSPWVD uses rearrangement to make the energy distribution closer to the ideal case. When the window function is narrow:

$$\int RSPWVD_x(t,f)df \approx |x(t)|^2 \quad (30)$$

Similarly, the frequency boundaries also satisfy:

$$\int RSPWVD_x(t,f)dt \approx |X(f)|^2 \quad (31)$$

Reordering effectively reduces the energy spread caused by smoothing windows, making the edge characteristics more consistent with the actual signal energy distribution.、

RSPWVD, with its ability to closely approximate the instantaneous frequency through the rearrangement of the $\hat{f}(t,f)$ coordinates, concentrates energy toward the center of the signal trajectory, significantly reducing the statistical variance of the time-frequency energy distribution and thereby substantially enhancing the focusing performance. At the same time, this method approximately restores the properties of the time and frequency edges. By performing a nonlinear remapping of energy, it mitigates the effects of multilevel smoothing inherent in smoothing windows, allowing the time-frequency profile to more accurately reflect the actual signal. These characteristics are crucial for analyzing multicomponent microseismic signals and non-stationary signals.

The floating-point operations of the RSPWVD are $O\left(c_1 \cdot N \cdot \tau_{max} \cdot L_g + c_2 \cdot N \cdot N_{fft} \cdot log_2 N_{fft} + c_3 \cdot N \cdot N_{fft}\right)$,where the maximum delay parameter $\tau_{\max} \approx min([N_{\text{fft}}/2], L_h)$, c_1 is the constant factor for the inner loop of the SPWVD, c_2 is the constant factor for the FFT, and c_3 is the constant factor for the reassignment.

3.3 Performance Comparison of Multi-Time-Frequency Analysis Methods

Under experimental conditions with two rotor blades, a blade length of 0.3 m, a rotational speed of 20 r/s, and a radar carrier frequency of 30 GHz, a rotor UAV echo model was established based on Equation (7),and the corresponding simulated echo signal was generated. The sampling frequency was set to 20 kHz to ensure that the Nyquist frequency was higher than the theoretical maximum micro-Doppler frequency of the simulated signal.Specifically, the Nyquist frequency is 10 kHz,

which is higher than the theoretical maximum micro-Doppler frequency of 7539.82 Hz. Therefore, the selected sampling frequency satisfies the Nyquist sampling criterion for the simulated micro-Doppler signal and avoids aliasing caused by an insufficient sampling rate.Four time-frequency analysis methods were used to analyze the signal generated based on the rotor UAV echo model, and the results are shown in Figure 3.

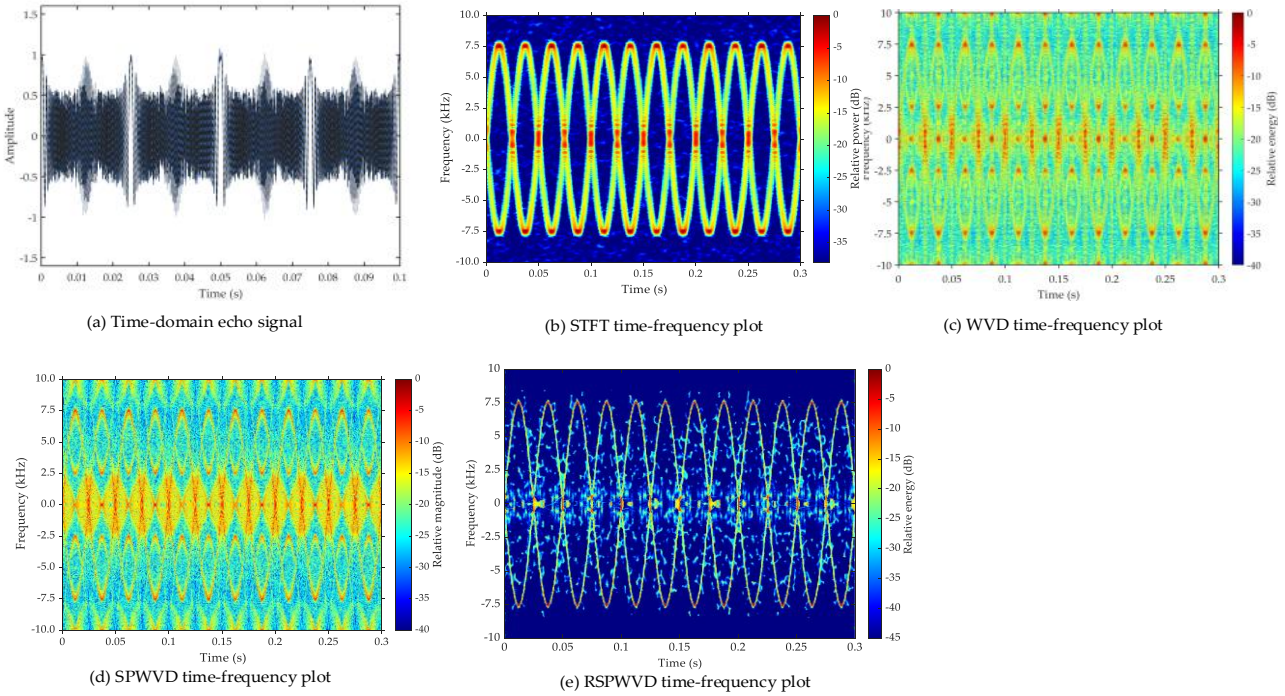

(a) Time-domain echo signal (b) STFT time-frequency plot (c) WVD time-frequency plot

(d) SPWVD time-frequency plot (e) RSPWVD time-frequency plot

Fig. 3. Time-frequency plot of a two-leaf echo

Table 1 compares the computational performance of v arious time-frequency analysis methods in terms of computational load (MFLOPs), execution time, and memory usage. The results show that RSPWVD consumes more computational resources than the other methods. However, as can be seen in Figure 3, the raw time-domain echo signal shown in Figure 3(a) can only reflect the variation of the echo amplitude over time; it cannot directly reveal the micro-Doppler modulation characteristics generated by the rotor blades, and therefore cannot effectively analyze micro-motion parameters. Figures 3(b)–3(e) present the time-frequency analysis results, STFT (Figure 3(b)) and RSPWVD (Figure 3(e)) can clearly characterize the periodic flickering bands generated by the rotation of the rotor blades, and their micro-Doppler frequency distributions are generally consistent with the theoretical analysis results. Due to the limitations of the fixed window function, the time-frequency focusing performance of the STFT is significantly inferior to that of the RSPWVD, whereas the RSPWVD provides a more concentrated time-frequency representation and better energy focusing through its rearrangement mechanism.

Indicators	STFT	WVD	SPWVD	RSPWVD
Computations / MFLOPs	59.584	58.113	67.560	209.000
Execution Time /ms	23.841	26.430	30.348	157.010
Memory Usage / MB	8.334	9.898	11.510	37.697

Table 1. Computational Complexity Analysis of Time-Frequency Analysis Algorithms

A comprehensive comparison shows that, although RSPWVD has a relatively high computational cost in terms of execution time and memory usage, it offers advantages in time-frequency resolution, energy concentration, and the ability to characterize micro-Doppler features, making it more suitable for the detailed analysis and parameter estimation of micro-

motion characteristics in rotorcraft drones.

A Method for Extracting Micro-Motion Characteristics of Low-Flying, Slow-Moving, Small UAV Rotors

Traditional feature extraction algorithms (such as EMD and SVD methods) are not very effective at extracting features from multi-component signals. Given that radar echoes from micro- and nano-UAVs are relatively weak, and that the randomness of the initial phases of different rotors in a multirotor configuration further complicates target identification, this section introduces CFD methods to achieve accurate extraction of micro-motion features from rotor-based UAVs, based on a comprehensive analysis of traditional micro-motion feature extraction techniques.

4.1 Cycle Frequency Diagram (CFD) Method

After obtaining the UAV radar echo signal, a sliding window of length N is first used to frame the echo sequence along the time axis, dividing the original signal into M adjacent data segments $\{\mathbf{x}_0, \mathbf{x}_1, \ldots, \mathbf{x}_{M-1}\}$, thereby constructing an $N \times M$ data matrix $\mathbf{S}$. For the i-th data window, its discrete Fourier transform $\mathbf{x}_i$ is expressed as:

$$\mathbf{X}_i = \mathbf{m}_i \exp\{j\boldsymbol{\theta}_i\} \tag{32}$$

where $\mathbf{m}_i$ and $\boldsymbol{\theta}_i$ represent the amplitude and phase information of the corresponding frequency component, respectively.

After obtaining the high-resolution time-frequency distribution of the UAV echo, the time-frequency matrix $\mathbf{R}_{RSPWVD}$ is acquired using the RSPWVD. Since the motion of the rotor blades is distinctly periodic, their micro-Doppler energy exhibits a repetitive distribution along the time axis. Therefore, a Fast Fourier Transform (FFT) can be further applied along the time dimension of the time-frequency matrix to map the periodic variations in the time domain to the Cadence Frequency domain, thereby obtaining the CFD spectrum. Its mathematical expression is:

$$\mathbf{CFD} = F_t\{\mathbf{R}_{RSPWVD}\} \tag{33}$$

where $\mathbf{R}_{RSPWVD} \in \square^{N_f \times N_t}$ is the RSPWVD time-frequency matrix, and F_t denotes the FFT operation along the time dimension.

From a signal processing perspective, the CFD method essentially performs spectral analysis on the time-varying energy sequences of each Doppler cell in a time-frequency plot. After the transformation, the Doppler frequency axis remains unchanged, while the time axis is converted to the Cadence Frequency axis, which is used to describe the repetitive periodic characteristics of each Doppler component. For rotor-based UAVs, the flickering phenomenon caused by the periodic rotation of the blades forms distinct spectral peaks in the cadence frequency dimension. Therefore, the CFD spectrum not only preserves the characteristics of the micro-Doppler frequency distribution but also highlights the periodic information of blade rotation, providing a more intuitive and stable representation of features for subsequent estimation of parameters such as blade flickering frequency, rotor speed, and blade length.

4.2 Estimation of Micro-Motion Parameters for Low-Altitude, Slow-Flying, Small Drones

For multi-component micro-Doppler signals, traditional peak-detection methods struggle to accurately estimate the microseismic parameters of each signal component. To improve the accuracy of parameter estimation, this paper employs a maximum-value estimation method, which extracts local energy peaks in the time-frequency domain to achieve effective separation and precise estimation of multi-component microseismic features.

For rotorcraft drones, when the radar beam is directed perpendicularly at the rotor blades, the radial velocity of the blade

tips along the radar line of sight reaches its maximum. At this point, the corresponding micro-Doppler frequency also reaches its maximum; therefore, the maximum Doppler frequency can be expressed as

$$f_{dmax} = \frac{4\pi f_{rot} L}{\lambda} \cos\beta \tag{34}$$

where λ is the radar wavelength, β is the elevation angle of the radar relative to the UAV's center of mass, L is the blade length, and f_{rot} is the rotor speed. In this paper, the estimation of f_{dmax} is performed directly in the RSPWVD time-frequency domain. After the echo signal undergoes time-frequency transformation, the local energy peaks of each signal component in the time-frequency plot correspond to the maxima in the time-frequency domain. Let $\mathbf{R}_{RSPWVD}(n,m)$ be a $N \times M$ dimensional RSPWVD time-frequency matrix. To suppress noise interference, the time-frequency matrix is first subjected to thresholding, and then a column-by-column search for maxima is performed, that is,

$$\boldsymbol{f}_1(:,i) = arg_{\,1 \leqslant i \leqslant M} \{\text{Peak}[\boldsymbol{R}_{RSPWVD}^{N \times M}(:,i)]\} \tag{35}$$

where $\mathbf{f}_1(:,i)$ represents the Doppler frequency corresponding to the location of the maximum value found in the i-th column, $\arg\{\cdot\}$ denotes the argument operation, and $Peak[\cdot]$ indicates the maximum value search.Therefore, the broadening of $\mathbf{f}_1$ in the frequency dimension can be used as an estimate of the maximum Doppler frequency $\hat{f}_{dmax}$, that is,

$$\hat{f}_{dmax} = \frac{|f_{1max} - f_{1min}|}{2} \tag{36}$$

where f_{1max} and f_{1min} correspond to the maximum and minimum Doppler frequencies of the signal components in $\mathbf{f}_1$, respectively.

This paper focuses on a two-blade rotor, where the blade flutter frequency is defined as the reciprocal of the time interval between two consecutive blade flutter events. The "Cadence Frequency" dimension in the CFD spectrum reflects the blade flutter frequency information; therefore, the same method used for the RSPWVD time-frequency matrix is employed to perform a column-by-column search for maxima in the CFD matrix, namely

$$\boldsymbol{f}_2(:,j) = arg_{\,1 \leqslant j \leqslant M} \{\text{Peak}[\boldsymbol{CFD}_{N \times M}(:,j)]\} \tag{37}$$

$\mathbf{f}_2(:,j)$ is the Doppler frequency corresponding to the location of the maximum value found in the j-th column. The interval between adjacent components of $\mathbf{f}_2$ in the Cadence Frequency dimension is the blade flash frequency $\hat{f}_{flash}$.Since a B times the rotor speed, that is,

$$\hat{f}_{rot} = \frac{\hat{f}_{flash}}{B} \tag{38}$$

For the two-blade rotor considered in this study, B=2. Overlapping flashes, unequal rotor speeds, missing blades, and asynchronous multirotor operation may violate this relationship and are not explicitly addressed in the present simulations.

Once the rotor speed $\hat{f}_{rot}$ and the maximum Doppler frequency $\hat{f}_{dmax}$ are known, the blade length can be further calculated.

$$\hat{L} = \frac{\hat{f}_{dmax} \lambda}{4\pi \hat{f}_{rot} \cos\beta} \tag{39}$$

Blade length is primarily determined by the rotor speed and the maximum Doppler frequency; once these two parameters have been estimated, the blade length can be calculated. Accurate estimation of key micro-motion parameters—such as rotor

speed and blade length—not only provides a crucial basis for UAV target detection and recognition but also offers effective parameter support for subsequent UAV type identification and target classification.

4.3 Algorithm and Procedure for Estimating Parameters of Low-Flying, Slow-Moving, Small UAVs Based on RSPWVD-CFD

The workflow for extracting micro-motion parameters of rotorcraft UAVs based on RSPWVD-CFD and maximum value estimation is shown in Figure 4. After acquiring the UAV's radar echo signal, the echo data is first subjected to fast time pulse compression processing; Subsequently, RSPWVD is applied to perform high-resolution time-frequency analysis of the signal, yielding a time-frequency matrix, and the maximum Doppler frequency is estimated using the local maxima of each component in the time-frequency plot; finally, an FFT is applied to the time-frequency matrix along the time dimension to obtain the CFD spectrum, from which blade flutter frequency information is extracted. This information is then combined with the maxi-mum Doppler frequency to estimate micro-motion parameters such as rotor speed and blade length.

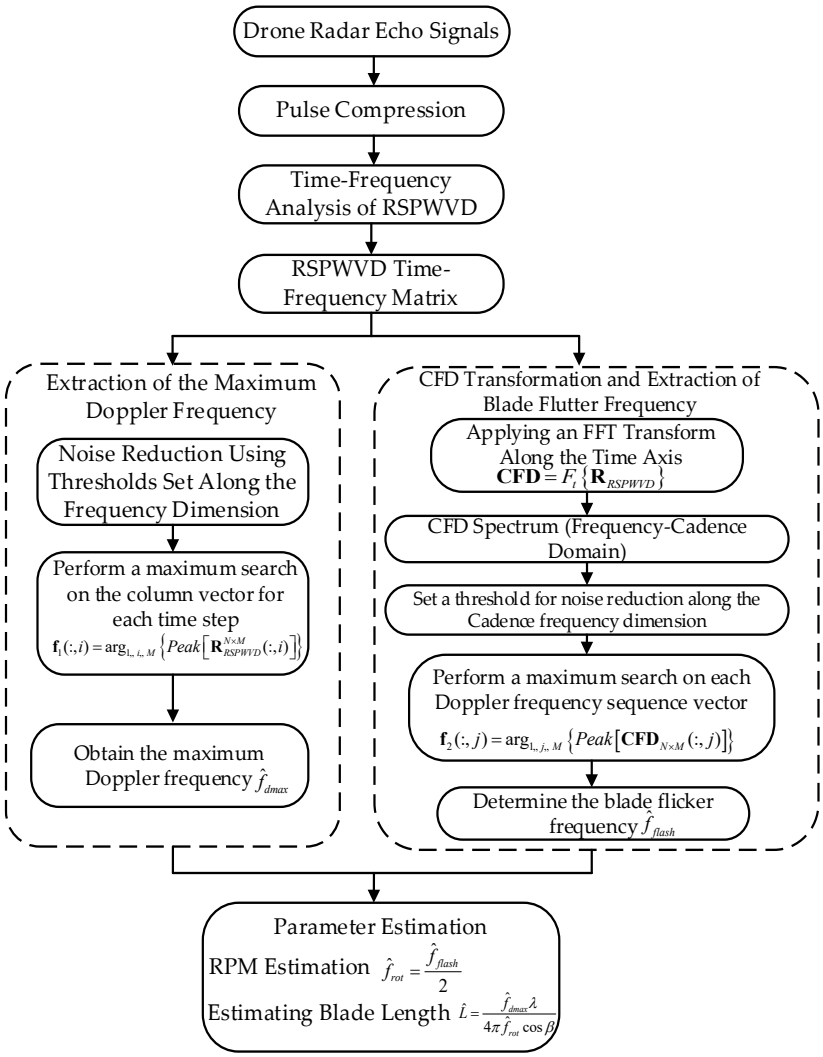

Fig.4 Block Diagram of Feature Extraction Using the RSPWVD-CFD Method

Traditional micro-motion feature extraction methods are susceptible to noise interference when processing echoes from low-flying, slow-moving, and small UAVs. At the same time, the randomness of the initial phase of multirotor blades can cause micro-Doppler features to overlap, making parameter estimation more difficult. Based on high-resolution time-frequency analysis using RSPWVD, this paper introduces CFD methods to extract periodic flutter features of the rotor blades,

thereby enabling effective estimation of key micro-vibration parameters and improving the accuracy and robustness of parameter extraction in complex scenarios.

To further clarify the implementation procedure of the proposed RSPWVD-CFD method, the main steps of micro-motion parameter estimation are summarized in Algorithm 1.

Algorithm 1: RSPWVD-CFD-Based Micro-Motion Parameter Estimation

Input: Radar echo signal $s(t)$; Radar wavelength lambda and pulse repetition frequency PRF;Elevation angle beta and number of blades $B = 2$; Time-frequency FFT size $N_{TF} = 1024$; Maximum lag $L_{max} = 96$samples; Time-smoothing window g and lag-smoothing window h; Energy threshold eta.

Output: Estimated rotor speed $\hat{f}_{\text{rot}}$; Estimated blade length $\hat{L}$.

1: Obtain the complex radar echo signal $s(t)$.

2: Calculate the smoothed pseudo-Wigner-Ville distribution (SPWVD) using the time-smoothing window g, lag-smoothing window h, and L_{max}.

3: Compute the time and frequency reassignment coordinates according to Equations (19) and (20).

4: Redistribute the SPWVD energy according to Equation (21) to obtain the RSPWVD matrix.

5: Apply energy threshold eta to suppress noise components in the RSPWVD matrix.

6: Perform column-wise local maximum search according to Equation (35) and estimate the maximum micro-Doppler frequency f_{dmax}using Equation (36).

7: Apply the FFT along the time dimension of the RSPWVD matrix to construct the cadence frequency diagram (CFD), as in Equation (33).

8: Estimate the blade-flash frequency $\hat{f}_{\text{flash}}$from the peak spacing along the cadence-frequency axis using Equation (37).

9: Estimate rotor speed using Equation (38): $\hat{f}_{\text{rot}} = \hat{f}_{\text{flash}}/B$.

10: Estimate blade length using Equation (39): $\hat{L} = \hat{f}_{d\text{max}}\lambda/4\pi\hat{f}_{\text{rot}}\,cos\,\beta$.

11: Return $\hat{f}_{\text{rot}}$and $\hat{L}$.

Results

To verify the effectiveness of the RSPWVD-CFD micro-motion parameter estimation method proposed in this paper, simulation experiments were conducted in three aspects: hovering state, motion state, and time-frequency analysis performance. First, under hovering conditions, the accuracy of the algorithm's estimates for parameters such as rotor speed, maximum micro-Doppler frequency, and blade length was verified. Subsequently, with the UAV in motion, the algorithm's adaptability to different motion states was further analyzed. Finally, RSPWVD was compared with typical time-frequency analysis methods such as STFT, WVD, and SPWVD to comprehensively evaluate the time-frequency resolution, energy concentration, and parameter estimation performance of each method.

5.1 Estimation of Micro-Motion Parameters for Rotorcraft Drones

To verify the parameter estimation capability of the RSPWVD-CFD method proposed in this paper under ideal conditions, simulation experiments were first conducted on a four-rotor, two-blade unmanned aerial vehicle (UAV) in a hovering state. The experiment employed a Ka-band linear frequency-modulated pulse radar system, with radar and target parameter settings as shown in Table 2. In the experiment, the initial phases of the four rotors were uniformly distributed between [-π , π], and the system signal-to-noise ratio was set to 25 dB. Figure 5 shows the results of the micro-motion parameter estimation for the quadcopter in hover.

Because the initial phases of the four rotors are random, there are slight differences in the flashing times corresponding to each rotor blade, and the flashing trajectories of some blades overlap; however, complete micro-Doppler trajectories can still be clearly observed in the RSPWVD time-frequency plot. According to theoretical analysis, the theoretical value of the maximum Doppler frequency is 4570.62 Hz. The maximum Doppler frequency estimated using the maximum value method is (4581.52 - (-4581.52)) / 2 = 4581.52 Hz. Since the rotational speeds of each rotor on a quadcopter in hover mode are identical, it has a unique flutter frequency. The theoretical value of the blade flutter frequency is 60 Hz, and Figure 5(d) shows an estimated blade flutter frequency of 60.04 Hz.

Parameter Name	Value
Carrier Frequency	35 GHz
Pulse Repetition Frequency	32 kHz
Fast-Time Sampling Frequency	500 MHz
Observation Duration	0.1 s
Rotor Speed	30 r/s
Scattering Coefficient	1
Blade Length	0.12 m
Distance Between UAV and Radar	1 km
UAV Body Speed	0
UAV Pitch Angle	π/6
UAV Azimuth Angle	0
Time-frequency FFT	1,024
Maximum lag	96 samples
Noise model	Complex Gaussian noise
Randomization	Independent phase with reproducible seeds

Table 2. Experimental Simulation Parameters

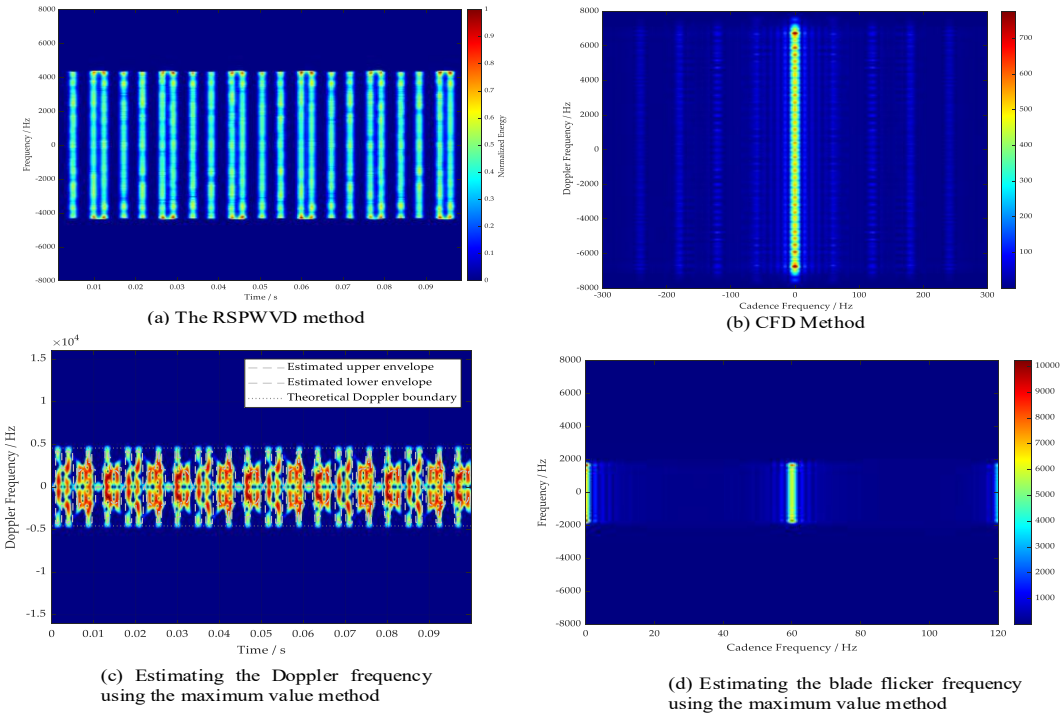

(a) The RSPWVD method

(b) CFD Method

(c) Estimating the Doppler frequency using the maximum value method

(d) Estimating the blade flicker frequency using the maximum value method

Fig.5 Estimation of Micro-Motion Parameters for a Quadcopter Drone

To further verify the stability of the algorithm, 100 Monte Carlo simulations were conducted while keeping all other parameters constant. In each simulation, the initial phases of the four rotors were randomly regenerated, and the estimation errors for rotor speed and blade length were calculated separately. The results are shown in Table 3, with relative root-mean-square errors of 0.25% for rotor speed and 2.65% for blade length. These results indicate that this method can accurately estimate the micro-motion parameters of a quadcopter.

Parameters	Actual value	Estimated value	Relative Root Mean Square Error	Standard Deviation
Rotational Speed	30 r/s	30.030 r/s	0.25%	0.0686 r/s
Blade Length	120 mm	119.100 mm	2.65%	3.0677 mm

Table 3 Calculated Results for Quadcopter Blade Length and Rotational Speed

To analyze the impact of different noise environments on algorithm performance, the signal-to-noise ratio (SNR) was set to values ranging from -10 dB to 25 dB. For each SNR value, 100 Monte Carlo simulations were conducted, ensuring that the initial phases of the four rotors were randomized in each simulation. The curves showing the variation of the relative root-mean-square error (RMSE) in the rotational speed and blade length of the quadcopter as a function of SNR are shown in Figure 6.

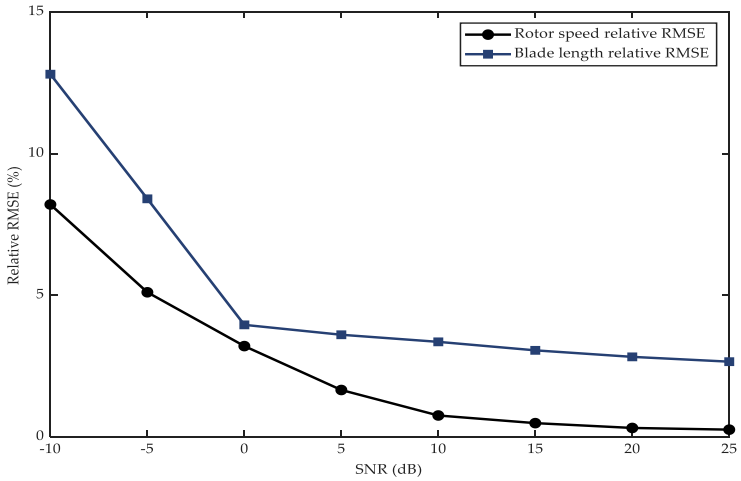

Fig.6. Performance Curves for the Estimation of Micro-motion Parameters of a Quadcopter UAV

As shown in Figure 6, when the signal-to-noise ratio is greater than 0 dB, the relative root-mean-square errors for both the rotational speed and blade length parameters are less than 4%; Although the errors increase in high-noise environments where the signal-to-noise ratio is below 0 dB,they decrease progressively as the SNR increases. This indicates that the RSPWVD-CFD method proposed in this paper exhibits good noise resistance and can maintain high parameter estimation accuracy even under moderate-to-high signal-to-noise ratio conditions.

5.2 Estimation of Micro-Motion Parameters for Rotorcraft UAVs in Motion

Next, simulation experiments were conducted on a four-rotor, two-blade UAV in flight. The UAV was assumed to be flying at a constant speed of 5 m/s in the direction of the radar line of sight, resulting in a Doppler shift of approximately 1166.67 Hz due to its translational motion. Other parameters are as shown in Table 2.

Due to the translational velocity of the UAV, the radar echo signal contains both the main translational Doppler component and the micro-Doppler modulation component caused by the rotors, resulting in a significant overall shift of the time-frequency trajectory in the Doppler frequency domain. Figure 7 shows the results of micro-Doppler parameter estimation for a quadcopter UAV in motion. As shown in Figure 7(a), the center of the micro-Doppler sinusoidal modulation trace has shifted upward from zero frequency to approximately 1166.67 Hz, and the RSPWVD method based on the rearrangement mechanism still achieves extremely high time-frequency coherence. Using the maximum value search method, the estimated maximum micro-Doppler frequency was determined to be 4581.52 Hz (the theoretical value is 4570.62 Hz). In the CFD spectrum, the micro-Doppler energy remains highly concentrated at a specific position on the flutter frequency axis. Figure 7(d) shows an estimated blade flutter frequency of 60.04 Hz, which closely matches the theoretical value of 60 Hz. Based on the relationship between the flutter frequency of a two-blade rotor and the rotational speed, the estimated rotor speed was calculated to be 30.02 r/s; by further combining this with the previously estimated maximum micro-Doppler frequency, the estimated blade length was ultimately calculated to be 120.18 mm in this representative trial.

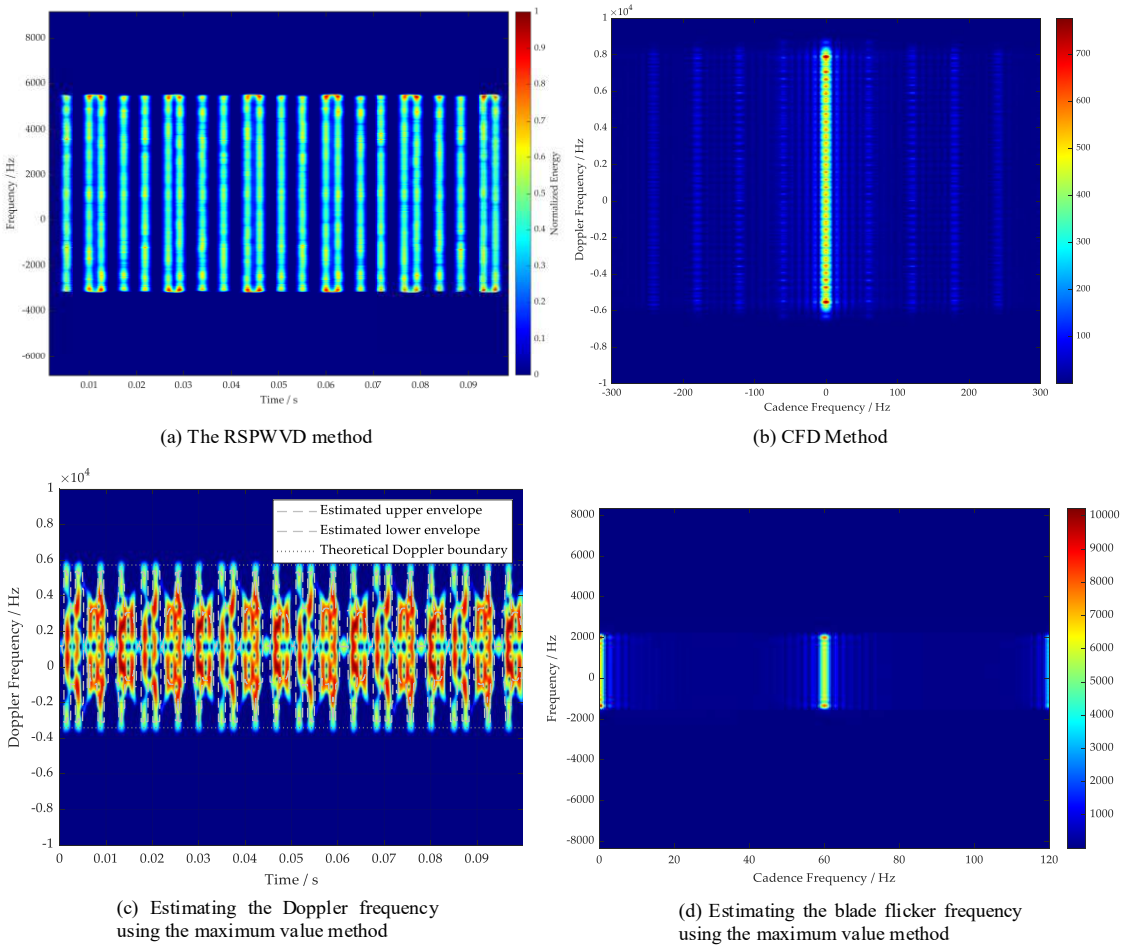

(a) The RSPWVD method

(b) CFD Method

(c) Estimating the Doppler frequency using the maximum value method

(d) Estimating the blade flicker frequency using the maximum value method

Fig. 7. Estimation of Micro-Motion Parameters for a Quadcopter UAV in Motion

The experimental results show that, despite significant translational Doppler shifts, the estimated flutter frequency of 60.04 Hz—along with parameters such as blade length—is highly consistent with the estimates obtained under hovering conditions. This is attributable to the relative search for maxima and the frequency-shift invariance of CFD, fully demonstrating that the algorithm exhibits exceptional robustness in feature extraction even under the interference of body motion.

To further verify the algorithm's stability, 100 Monte Carlo simulations were conducted while keeping all other parameters constant. In each simulation, the initial phases of the four rotors were randomly regenerated, and the estimation errors for rotor speed and blade length were calculated separately. The experimental results are shown in Table 4, with relative root-mean-square errors (RMSE) of 0.38% for rotor speed and 3.12% for blade length. These results demonstrate that this method can accurately estimate the micro-motion parameters of a quadcopter UAV.

Parameters	Actual value	Estimated value	Relative Root Mean Square Error	Standard Deviation
Rotational Speed	30 r/s	30.045 r/s	0.38%	0.1050 r/s
Blade Length	120 mm	118.800 mm	3.12%	3.5559 mm

Table 4 Calculated Results for Quadcopter Blade Length and Rotational Speed

To analyze the impact of different noise environments on algorithm performance, the signal-to-noise ratio (SNR) was set to values ranging from -10 dB to 25 dB. For each SNR value, 100 Monte Carlo simulations were conducted, ensuring that the initial phases of the four rotors were randomized in each simulation. The curves showing the variation of the relative root-

mean-square error (RMSE) of the quadcopter's rotational speed and blade length as a function of SNR are shown in Figure 8.

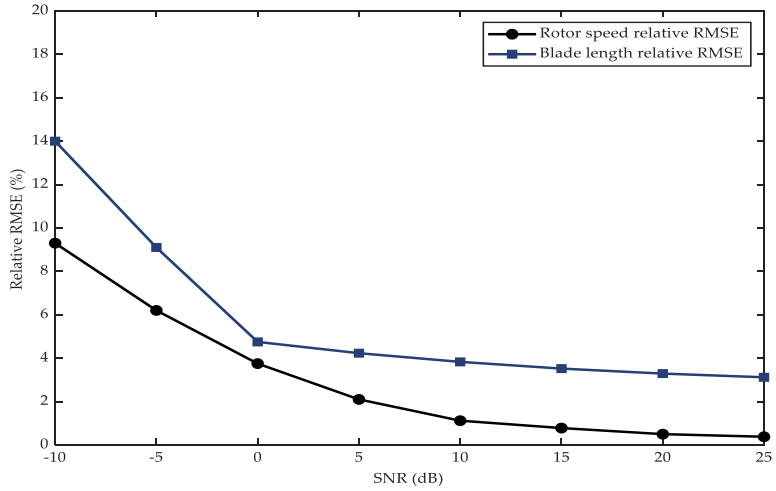

Fig. 8. Performance Curves for the Estimation of Micro-motion Parameters of a Quadcopter UAV in Motion

As shown in Figure 8, after introducing translational disturbance, the trend in parameter estimation accuracy as the signal-to-noise ratio (SNR) varies is essentially consistent with that in the hovering state. Although the estimation errors are slightly higher than those under hovering conditions,when the SNR is greater than 0 dB, the relative root-mean-square errors for both the rotational speed and blade length parameters are less than 6%. The results indicate that the RSPWVD-CFD method maintains its parameter-estimation capability under the simulated constant-velocity motion conditions.

5.3 Time-Frequency Analysis Results for a Two-Blade Rotor UAV

To verify the time-frequency analysis performance of the RSPWVD method adopted in this paper, time-frequency analyses of the echoes from a quadcopter with two blades per rotor were performed under identical experimental conditions using STFT, WVD, SPWVD, and RSPWVD, respectively. The corresponding results are shown in Figure 9, and a comparison of the performance of each method is presented in Table 5. As shown in Figure 9, STFT has low time-frequency resolution due to the limitations of its fixed window function, resulting in significant broadening of the micro-Doppler trajectories. WVD has high theoretical resolution, but severe cross-terms cause a large number of artifacts in the time-frequency plot, making it difficult to accurately extract the true micro-Doppler trajectories. Although SPWVD can suppress cross-terms to some extent, the time-frequency smoothing process leads to energy diffusion, causing blurred trajectory edges. In contrast, RSPWVD utilizes a rearrangement mechanism to redistribute energy, effectively suppressing cross-terms while significantly improving time-frequency coherence. The micro-Doppler trajectories are continuous and clear, which is more conducive to subsequent peak search and CFD parameter extraction.

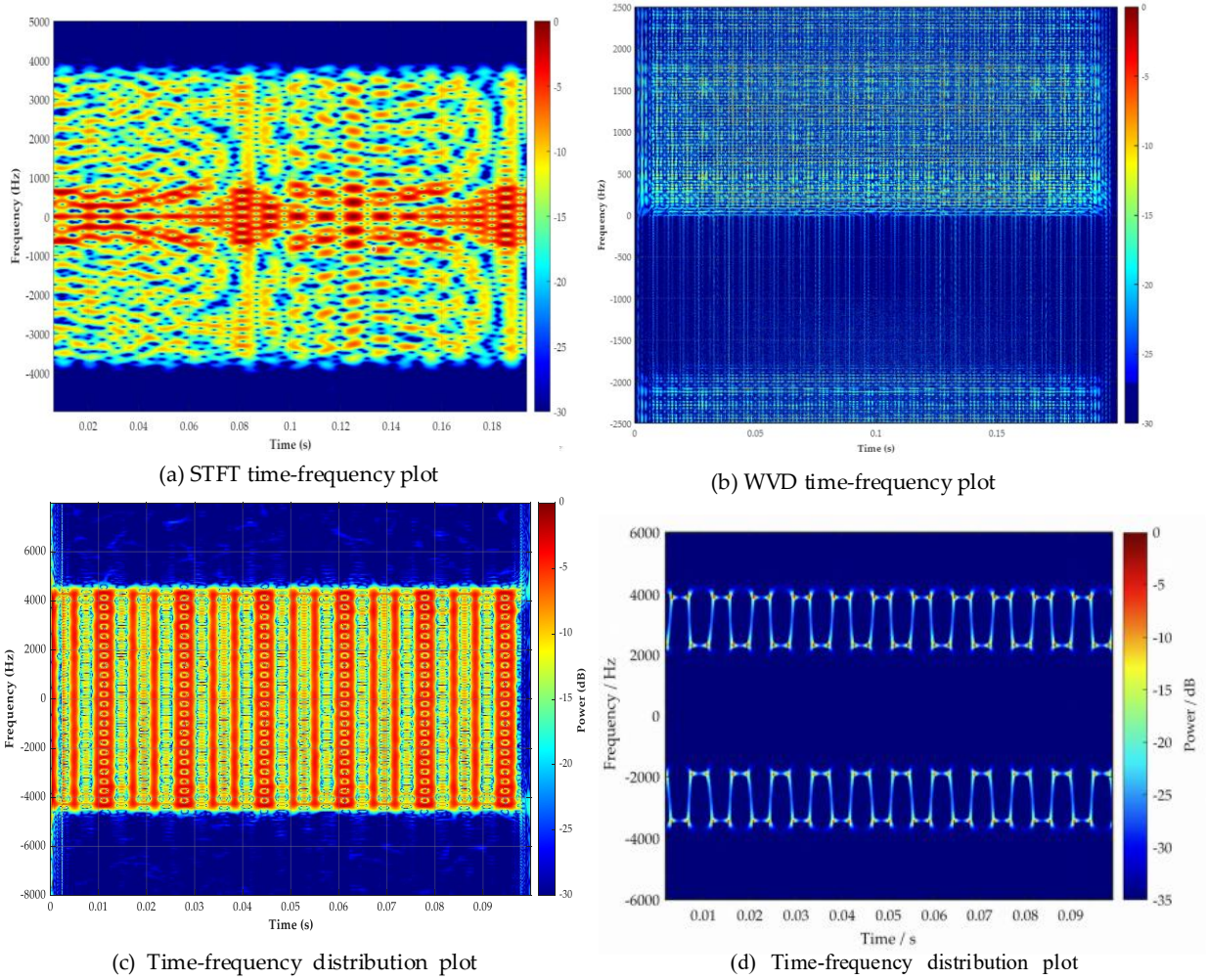

(a) STFT time-frequency plot

(b) WVD time-frequency plot

(c) Time-frequency distribution plot for SPWVD

(d) Time-frequency distribution plot for RSPWVD

Fig. 9. Time-frequency plot of a twin-blade quadcopter

Here, the normalized standard deviation σ_{norm} measures time-frequency energy concentration, while the time-frequency resolution factor R_{tf} evaluates resolution relative to the theoretical limit; lower values of both metrics indicate better performance.

Indicators	STFT	WVD	SPWVD	RSPWVD
σ_{norm}	0.118	0.164	0.093	0.071
R_{tf}	38.420	11.637	6.284	2.913

Table 5. Time-Frequency Analysis Metrics for a Two-Blade Quadcopter

According to the results in Table 5,RSPWVD has the smallest normalized standard deviation (0.071), indicating the strongest energy concentration among the compared methods; it also achieves the resolution factor (2.913) closest to the ideal value of 1, suggesting improved time-frequency resolution. However, as shown in the time-frequency distribution plot in Figure 9, the WVD suffers from significant cross-term interference, resulting in blurred frequency-shifted stripes and artifacts, while the STFT, limited by its fixed window function, has lower time-frequency resolution and cannot clearly separate dense micro-Doppler components. RSPWVD performs well in terms of both normalized standard deviation (0.071) and resolution factor (2.913). Furthermore, through rearrangement operations, it significantly suppresses interference terms; the time-frequency plot exhibits clear stripe structures and good feature continuity, making it more suitable for extracting the complex

micro-vibration characteristics of quadcopter drones.The two metrics favor RSPWVD in this illustrative comparison; however, quantitative evaluation of cross-term suppression, trajectory accuracy, parameter estimation errors, and computational cost remains necessary to establish its overall superiority.

Conclusion

To address the issues of micro-Doppler characteristics of rotorcraft UAV radar echoes being susceptible to noise interference in low signal-to-noise ratio environments and the difficulty in accurately estimating key micro-motion parameters, this paper proposes a method for estimating micro-motion parameters of rotorcraft UAVs based on RSPWVD-CFD. The main conclusions are as follows:

(1) A dynamic radar echo model was established that accounts for the UAV's spatial geometry, rotor micro-vibrations, and the effects of the main body's translational motion. This model accurately describes the micro-Doppler modulation characteristics of the rotor, providing a theoretical foundation for high-resolution time-frequency analysis and the estimation of micro-vibration parameters.

(2) An RSPWVD-CFD-based method for estimating micro-Doppler parameters was proposed. RSPWVD was used to enhance time-frequency energy concentration and suppress interference from cross-terms, while CFD was employed to extract the blade flutter frequency. The maximum micro-Doppler frequency was estimated via a maximum value search, enabling the inversion of rotor speed and blade length. Simulation results show that, at 25 dB SNR, the reported relative root-mean-square errors for rotational speed and blade length are 0.25% and 2.65% under hovering conditions and 0.38% and 3.12% under constant-velocity motion, respectively; when the SNR exceeds 0 dB, both errors remain below 4% for hovering and 6% for moving conditions. Compared with STFT, WVD, and SPWVD, RSPWVD yields clearer and more continuous micro-Doppler trajectories, providing higher-quality time-frequency input for parameter estimation.

This paper verifies the effectiveness of the proposed method under simulation conditions; however, its adaptability to complex electromagnetic environments and real radar data requires further study. Future work will involve field validation using actual measurement data and further research into micro-Doppler parameter estimation and real-time processing methods in complex scenarios to enhance the algorithm's engineering applicability.

Funding.

2025 Shaanxi Provincial Department of Education Scientific Research Project Plan (Grant No. 25JK0593).

Disclosures.

The authors declare no conflicts of interest.

Data availability.

The datasets used and/or analysed during the current study are available from the corresponding author on reasonable request.

Reference

1. Zhang, J.; Zhang, K.; Wang, J.Y.; Li, B. Current status and development trend of low-altitude anti-UAV technology[J]. * Progress in Aerospace Engineering *,2018, 9, 1–8. DOI:10.16615/j.cnki.1674-8190.2018.01.001 (In Chinese)
2. Chen, V.C. The Micro-Doppler Effect in Radar; Artech House: London, UK, 2011.
3. Zhao, X.C.; Zhao, D.T.; Yuan, H.; Zhang, L.R.; Liu, X.; Luo, D.L. Micro-motion parameter extraction of UAV under low pulse repetition frequency[J]. * Systems Engineering and Electronics *,2024, 46, 1503–1513. doi:10.12305/j.issn.1001-506X.2024.05.05 (In Chinese)
4. Jiu, B.; Zhang, L.; Wu, S.J. Progress and prospect of radar detection and recognition technology for birds and UAV targets[J]. * Journal of Radars *,2020, 9, 115–131. doi:10.12000/JR20068 (In Chinese)
5. He, W.K.; Sun, J.B.; Zhang, X.Y.; Xue, Y.S. Micro-Doppler feature extraction of micro-rotor UAV under the background of low SNR[J]. * Journal of Systems Engineering and Electronics *,2022, 33, 1127–1139. DOI:10.23919/JSEE.2022.000138

6. Tang, M.L.; Zhang, W.P.; Jiang, W.D.; Liu, Z.; Xue, F. Micro-motion signal enhancement method based on multi-resolution saliency filtering[J]. * Systems Engineering and Electronics *,2022, 44, 1148–1157. doi:10.12305/j.issn.1001-506X.2022.04.10 (In Chinese)
7. Chen, V.C. Analysis of radar micro-Doppler with time-frequency transform[J]. * In Proceedings of the 10th IEEE Workshop on Statistical Signal and Array Processing, Pocono Manor, PA, USA, 14–16 August*,2000; pp. 463–466. DOI:10.1109/SSAP.2000.870167
8. Cohen, L. Time-Frequency Analysis; Prentice Hall: New Jersey, NJ, USA, 1995. DOI:10.1016/B978-0-08-044335-5.X5020-7
9. Claasen, T.A.C.M.; Mecklenbräuker, W.F.G. The Wigner distribution—A tool for time-frequency signal analysis[J]. * Philips Journal of Research *,1980, 35, 217–250.
10. Whitelonis, N.; Ling, H. Radar signature analysis using a joint time-frequency distribution based on compressed sensing[J]. * IEEE Transactions on Antennas and Propagation*, 2014, 62, 755–763. DOI:10.1109/TAP.2013.2291893
11. Ram, S.S.; Ling, H. Analysis of micro-Dopplers from human gait using reassigned joint time-frequency transform[J]. * Electronics Letters *,2007, 43, 1309–1311. DOI:10.1049/el:20071515
12. Wei, Q.G.; Wu, J.H. Reassignment method of time-frequency analysis for non-stationary signals and its application in speech signal processing[J]. * Journal of Nanchang University (Natural Science Edition) *,2004, 28, 74–77. (In Chinese)
13. Auger, F.; Flandrin, P. Improving the readability of time-frequency and time-scale representations by the reassignment method[J]. * IEEE Transactions on Signal Processing *,1995, 43, 1068–1089. DOI:10.1109/78.382394
14. Daubechies, I.; Lu, J.; Wu, H.T. Synchrosqueezing wavelet transforms: An empirical mode decomposition-like tool[J]. * Applied and Computational Harmonic Analysis *,2011, 30, 243–261. DOI:10.1016/j.acha.2010.08.002
15. Yu, G.; Zhou, Y. Synchroextracting transform[J]. * IEEE Transactions on Industrial Electronics*, 2017, 64, 9442–9452. DOI:10.1109/TIE.2017.2696503
16. Boashash, B. Time-Frequency Signal Analysis and Processing[J]. * A Comprehensive Reference; Elsevier: Amsterdam, The Netherlands*,2015.
17. Oh, B.S.; Guo, X.; Wan, F.; Tan, V.S.; Toh, K.A. An EMD-based micro-Doppler signature analysis for mini-UAV blade flash reconstruction[J]. * In Proceedings of the 2017 22nd International Conference on Digital Signal Processing (DSP), London, UK, 23–25 August *,2017. DOI:10.1109/ICDSP.2017.8096105
18. Zhang, W.Y.; Li, G. Detection of multiple micro-drones via cadence velocity diagram analysis[J]. * Electronics Letters *,2018, 54, 441–443. DOI:10.1049/el.2017.4317
19. Xia, S.Q.; Zhu, M.S.; Chen, W.F.; Wan, X.R.; Yi, J.X. Micro-motion feature extraction method of rotor based on flash phenomenon[J]. * Radar Science and Technology *,2019, 17, 671–678. DOI:10.3969/j.issn.1672-2337.2019.06.014 (In Chinese)
20. He, W.K.; Sun, J.B.; Wang, X.L.; Zhang, X.Y. Micro-motion feature extraction of small rotor UAV based on RSP-CFD method[J]. * Journal of Signal Processing *,2021, 37, 399–408. DOI:10.16798/j.issn.1003-0530.2021.03.010 (In Chinese)
21. Chen, X.K.; Wang, X.R.; Huang, X.H. Rotor parameter estimation of low-slow-small UAV based on TELSET[J]. * Journal of Signal Processing *,2026, 42, 843–856. DOI:10.12466/xhcl.2026.06.006 (In Chinese)
22. Ge, L.H.; Li, K.; Liu, S.J.; Liang, Y.; Xing, M.D. Research on UAV recognition based on RSPWVD reassigned spectrogram algorithm[J]. * Systems Engineering and Electronics *,2026. Available online:

https://link.cnki.net/urlid/11.2422.TN.20260427.1617.004 (accessed on 13 July 2026). (In Chinese)

23. LeCun, Y.; Bengio, Y.; Hinton, G. Deep learning[J]. * Nature *,2015, 521, 436–444. DOI:10.1038/nature14539
24. Krizhevsky, A.; Sutskever, I.; Hinton, G.E. ImageNet classification with deep convolutional neural networks[J]. * Communications of the ACM *,2017, 60, 84–90. DOI:10.1145/3065386
25. Redmon, J.; Divvala, S.; Girshick, R.; Farhadi, A. You only look once: Unified, real-time object detection[J]. * In Proceedings of the IEEE Conference on Computer Vision and Pattern Recognition (CVPR), Las Vegas, NV, USA, 27–30 June *,2016; pp. 779–788. DOI:10.1109/CVPR.2016.91
26. Park, D.; Lee, S.; Park, S.U.; Kim, S. Radar-Spectrogram-Based UAV Classification Using Convolutional Neural Networks[J]. * Sensors *,2021, 21, 21010210. DOI:10.3390/s21010210
27. Huang, W.; Guo, H.; Li, X.; Wang, X. Research on optimized YOLOv5s algorithm for detecting aircraft landing runway markings[J]. * Processes *,2025, 13, 2572. DOI:10.3390/pr13082572
28. Xu, W.; Zhang, H.; Zhang, Y.; Liu, K.; Zhang, J.; Zhu, Y.; Dilixiati, B.; Ning, J.; Gao, J. YOLO-DS: a detection model for desert shrub identification and coverage estimation in UAV remote sensing[J]. * Journal of Forestry Research *,2025, 36, 116. DOI:10.1007/s11676-025-01916-w
29. Yin, S.; Xiang, Z. Energy-constrained collaborative path planning for heterogeneous amphibious unmanned surface vehicles in obstacle-cluttered environments[J]. * Ocean Engineering *,2025, 330, 121241. DOI:10.1016/j.oceaneng.2025.121241.
30. Yin, S.; Hu, J.; Xiang, Z. Multi-objective collaborative path planning for multiple water-air unmanned vehicles in cramped environments[J]. * Expert Systems with Applications *,2025, 292, 128625. DOI:10.1016/j.eswa.2025.128625.
31. Yin, S.; Chen, X.; Zhang, Y.; Xiang, Z. Cooperative multi-USV coverage scheduling in obstacle-rich waters: A DRL-assisted adaptive evolutionary approach[J]. * Expert Systems with Applications*,2027, 332, 133648. DOI:10.1016/j.eswa.2026.133648.